CHEMISTRY OF MATERIALS
Article

Chem. Mater. **2009,** *21,* 2607–2613 2607
DOI:10.1021/cm802022p

Synthesis of Ternary $CuInS_2$ Nanocrystals; Phase Determination by Complex Ligand Species

Katsuhiro Nose, Yuki Soma, Takahisa Omata,* and Shinya Otsuka-Yao-Matsuo

Division of Materials and Manufacturing Science, Graduate School of Engineering, Osaka University, 2-1 Yamada-oka, Suita, 565-0871 Japan

Received July 25, 2008. Revised Manuscript Received April 27, 2009

Colloidal $CuInS_2$ nanocrystals were synthesized in a hot organic solvent containing surfactant molecules. The $CuInS_2$ phase was controlled by the ligand species of the metallic monomers. When the metallic monomers were coordinated with trioctylphosphite, the resulting $CuInS_2$ had a chalcopyrite or zincblende phase. When the metallic monomers were coordinated with hexadecylamine or oleylamine, the thermodynamically metastable wurtzite phase appeared. The experimental results indicated that the obtained phase was predominantly determined by the growth rate of the nanocrystals. The bond strength between the metallic monomers and ligand molecules and steric size of the ligand molecules influenced the growth rate. The $CuInS_2$ nanocrystals showed photoluminescence in the near-infrared region. Its energy was far from the optical energy band gap; the luminescence was attributable to the electron−hole recombination via deep defect levels. In the photoluminescence spectrum of the $CuInS_2$/ZnS core/shell nanocrystals, a band near the optical energy band gap, whose Stokes' shift was ∼50 meV, appeared. The band was suggested to be attributable to the defect-related emission from $CuInS_2$−ZnS alloy formed at the interfaces between the core $CuInS_2$ and shell ZnS.

Introduction

Direct-transition compound semiconductors are very attractive materials because of their variety of applications in optoelectronic devices such as solar cells and light-emitting devices. Semiconductor nanocrystals (NCs) possessing several nanometer diameters, which are termed quantum dots, show a widening of their optical energy band gap upon decreasing their crystal size because of the quantum size effect, i.e., the optical absorption and photoluminescence (PL) wavelength are adjustable by control of their crystal size.[1] Therefore, the direct-transition semiconductor NCs are expected to be utilized for the advanced optoelectronic application of quantum dot light emitting devices[2−7] and quantum dot solar cells.[8] Among the compound semiconductors, CdSe is a promising material for such applications because of its established synthetic chemistry of achieving high-quality NCs.[1] However, their use in practical applications is limited because of the cadmium and selenium toxicity. To develop low-toxicity or less-toxic direct-transition semiconductor NCs as alternatives to the CdSe is now strongly demanded.

Ternary $CuInS_2$ with a chalcopyrite structure is a direct transition semiconductor possessing a 1.53 eV energy band gap,[9] and it is composed of less toxic elements. $CuInS_2$ is a hopeful candidate as an alternative to CdSe. Several synthesis attempts have been reported of the $CuInS_2$ NCs.[10−15] For example, Castro et al. successfully synthesized $CuInS_2$ NCs by thermolysis of the molecular single-source precursor $(PPh_3)_2CuIn(SEt)_4$ and observed the red PL from the NCs.[11] However, their PL was not attributable to the exciton-recombination but to the electron−hole recombination via deep defect levels. The energy of the PL arising from the deep levels is much lower than the optical energy band gap, i.e., the deep level

*Corresponding author. Tel: 81-6879-7462 or 81-6879-7463. fax: 81-6879-7464. E-mail: omata@mat.eng.osaka-u.ac.jp.

(1) Murray, C. B.; Norris, D. J.; Bawendi, M. G. *J. Am. Chem. Soc.* **1993**, *115*, 8706.
(2) Mattoussi, H.; Radzilowski, L. H.; Dabbousi, B. O.; Thomas, E. L.; Bawendi, M. G.; Rubner, M. F. *J. Appl. Phys.* **1998**, *83*, 7965.
(3) Rizzo, A.; Li, Y.; Kudera, S.; Sala, F. D.; Zanella, M.; Parak, W. J.; Cingolani, R.; Manna, L.; Gigli, G. *Appl. Phys. Let.* **2007**, *90*, 051106.
(4) Kobayashi, S.; Tani, Y.; Kawazoe, H. *Jpn. J. Appl. Phys.* **2007**, *46*, L392.
(5) Achermann, M.; Petruska, M. A.; Kos, S.; Smith, D. L.; Koleske, D. D.; Klimov, V. I. *Nature* **2004**, *429*, 642.
(6) Sullivan, S. C.; Woo, W. K.; Steckel, J. S.; Bawendi, M.; Bulovic, V. *Org. Elect.* **2003**, *4*, 123.
(7) Cham, Y.; Steckel, J. S.; Snee, P. T.; Caruge, J. M.; Hodgkiss, J. M.; Nocera, D. G.; Bawendi, M. G. *Appl. Phys. Let.* **2005**, *86*, 073102.
(8) Raffaella, R.; Castro, S. L.; Hepp, A. F.; Gailey, S. G. *Prog. Photovoltaics: Res. Appl.* **2002**, *10*, 433.
(9) Tell, B.; Shay, J. L.; Kasper, H. M. *Phys. Rev. B* **1971**, *4*, 2463.
(10) Castro, S. L.; Bailey, S. G.; Raffaella, R. P.; Banger, K. K.; Hepp, A. F. *Chem. Mater.* **2003**, *15*, 3142.
(11) Castro, S. L.; Bailey, S. G.; Raffaella, R. P.; Banger, K. K.; Hepp, A. F. *J. Phys. Chem. B* **2004**, *108*, 12429.
(12) Nairn, J. J.; Shapiro, P. J.; Twamley, B.; Pounds, T.; Wandruszka, R.; Fletcher, T. R.; Williams, M.; Wang, C.; Norton, M. G. *Nano Lett.* **2006**, *6*, 1218.
(13) Xiao, J.; Xie, Y.; Tang, R.; Qian, Y. *J. Solid State Chem.* **2001**, *161*, 179.
(14) Xiao, J.; Xie, Y.; Tang, R.; Qian, Y. *J. Mater. Chem.* **2001**, *11*, 1417.
(15) Czekelius, C.; Hilgendorff, M.; Spanhel, L.; Bedja, I.; Lerch, M.; Müller, G.; Bloeck, U.; Su, D. -S.; Giersig, M. *Adv. Mater.* **1999**, *11*, 643.

Published on Web 05/19/2009

PL shows a large Stokes' shift; therefore, the luminescence is inefficient when the energy of the luminescence is compared to that of the excitation. When the NCs are used in solar cells, the deep levels behave as recombination centers decreasing the solar cell efficiency. To attain an energy-efficient luminescence and high solar cell efficiency, achieving the PL arising from the exciton-recombination, whose Stokes' shift is generally lower than 100 meV for the semiconductor NCs, is necessary. Although the visible PL from less-toxic semiconductor NCs has also been reported in quaternary ZnS-$CuInS_2$ [16] and ZnS-$AgInS_2$ [17] NCs, the PL arising from the exciton recombination has not yet been reported for those NCs. Understanding the synthetic chemistry of the $CuInS_2$ NCs and developing high-quality $CuInS_2$ NCs are important issues in order to realize practically applicable semiconductor NCs.

We now report the synthesis of colloidal $CuInS_2$ NCs using simple and commercially available reagents as the starting materials and optical properties of the $CuInS_2$ and $CuInS_2$/ZnS core/shell NCs. During the synthesis, we observed a phenomenon that is a phase transformation of $CuInS_2$ depending on the time after the addition of the surfactant amine; very recently, a similar phase transformation of $CuInS_2$ was reported by Pan et al.[18] The phase transformation was studied by infrared (IR) spectroscopy of the reaction solution and X-ray diffraction (XRD). The mechanism was explained in terms of the nucleation and crystal growth rates determined by the ligand species of the metallic monomers. In the PL spectrum of the $CuInS_2$/ZnS core/shell NCs, a PL band near the optical energy band gap, whose Stokes' shift was approximately 50 meV, was successfully observed. The PL was suggested to occur from the exciton recombination.

Experimental Section

Materials. Copper iodide (CuI, 98.0%, Kishida Chemicals), indium chloride anhydrous ($InCl_3$, 99.0%, Kishida Chemicals), sulfur powder (Aldrich, reagent grade), tri-n-octylphosphine (TOP, Tokyo Chemical Industry), trioctylphosphite (TOOP, >98%, Tokyo Chemical Industry), triphenylphosphite (TPOP, >95%, Tokyo Chemical Industry), 1-octadecene (ODE, >90%, Tokyo Chemical Industry), 1-hexadecylamine (HDA, 90%, Aldrich), oleylamine (OLA, Aldrich, 70%), ethanol (Sigma-Aldrich Japan, >99.5%), hexane (Sigma-Aldrich, >99%), chloroform (Sigma-Aldrich Japan, >99.8%), and zinc diethyldithiocarbamate (>99%, Tokyo Chemical Industry) were commercially available. The OLA was purified by distillation before use. All other chemicals were used without further purification. The carbon-coated copper grid (200-mesh) for preparing the TEM specimens was purchased from Okenshoji.

Synthesis of Colloidal $CuInS_2$ and $CuInS_2$/ZnS Core/Shell NCs. The $CuInS_2$ NCs were synthesized by the following procedures. A copper source solution was prepared by dissolving 38.1 mg of CuI in a mixed solvent of 282 μL of TOOP and 5.0 mL of ODE at 180 °C for 40 min and then cooling to room temperature. An indium source solution was prepared by dissolving 221.2 mg of $InCl_3$ in 1.0 mL of TOOP at 140 °C for 60 min under flowing argon and then cooling to room temperature. The $InCl_3$ in the TOOP solution was diluted with 4.0 mL of ODE, and 1 mL of the $InCl_3$ in the TOOP and ODE solution was again diluted with 4 mL of ODE. A sulfur solution was prepared by dissolving 77.0 mg of sulfur powder in 5 mL of TPOP at 120 °C for 40 min. A 1.0 mL aliquot of the respective source solutions were mixed in a glass vial (12 mL capacity), and 0.5 mmol of HDA or OLA was added. The resulting solution was called the starting solution. After the starting solution was stored at room temperature for 3 min or 3 h, the starting solution in a glass vial was placed in an oil-bath maintained at 200−240 °C. The vial was rapidly removed from the oil-bath after the predetermined reaction time (30 s to 5 min), and then cooled to room temperature.

The $CuInS_2$/ZnS core/shell NCs were synthesized by the following procedures. Zinc diethyldithiocarbamate (90.5 mg) was dissolved into 3 mL of TOP at room temperature. A 7.7 mL aliquot of ODE and 106 μL of OLA were added to the zinc diethyldithiocarbamate TOP solution; this solution was the ZnS source solution. The $CuInS_2$ NCs extracted from 3 mL of the product solution were dispersed in the 3 mL of the ZnS source solution, and then the solution was reacted at 200 °C for 30 min. All the preparation procedures and the reactions were carried out under an Ar atmosphere and without any stirring and agitation. However, Ar-gas was bubbling during the synthesis; it strongly stirred the reaction solution.

Characterization. The obtained crystalline phases were identified using powder X-ray diffraction (XRD) (Rigaku, RINT2500, Cu Kα radiation using a curved graphite receiving monochromator). The powdered samples were extracted from the product colloidal solution by the following procedure. One milliliter of hexane was added to a 1 mL aliquot of the product colloidal solution, and ethanol was then added until the NCs aggregated. The aggregated NCs were isolated by centrifugation and decantation. These procedures were repeated several times, and the resulting wet precipitate was dried under vacuum at room temperature. The average crystal size was evaluated from the full-width at half-maximum of the XRD peaks using the Debye−Scherrer equation.

Infrared absorption spectra of the solutions were recorded in the transmission mode at room temperature by a Fourier transform infrared spectrometer (FT/IR-610 V, JASCO) with a deuterated L-alanine triglycine sulfate (DLATGS) detector. The specimen solution was loaded into the press-on demountable liquid cell with KBr windows (PIKE Technologies, Inc.); a 0.1 mm thick spacer was used as needed.

The UV−visible absorption spectra were recorded by a Hitachi U4000 spectrophotometer. The photoluminescence (PL) spectra were acquired using an USB2000 spectrometer (Ocean Optics) with a diode-pumped solid-state (DPSS) laser (Shanghai Sanctity Laser Technology Co., Ltd.) at a wavelength of 473 nm as the excitation source. The product NCs, which were extracted from a 1.0 mL aliquot of the product solution, were redispersed in 3 mL of chloroform. It was loaded into the standard fluorometer cells made of SiO_2 glass, whose optical path length was 10 mm, which was then subjected to the UV−visible absorption and PL spectroscopies. The obtained PL spectra were corrected for the wavelength dependence of the detector.

A scanning electron microprobe (JEOL, JSM-5600) operated at 15 kV was used to determine the chemical composition of the

(16) Nakamura, H.; Kato, W.; Uehara, M.; Nose, K.; Omata, T.; Otsuka-Yao-Matsuo, S.; Miyazaki, M.; Maeda, H. *Chem. Mater.* **2006**, *18*, 3330.
(17) Torimoto, T.; Adachi, T.; Okazaki, K.; Sakuraoka, M. Shibayama, T.; Ohtani, B.; Kudo, A.; Kuwabata, S. *J. Am. Chem. Soc.* **2007**, *129*, 12388.
(18) Pan, D.; An, L.; Sun, Z.; Hou, W.; Yang, Y.; Yang, Z.; Lu, Y. *J. Am. Chem. Soc.* **2007**, *130*, 5620.

product NCs using energy-dispersive X-ray (EDX) spectroscopy (EDAX, CDU-S). For the SEM and EDX measurements, the powdered samples were placed on a titanium plate. High-resolution transmission micrographs were obtained by a JEOL JEM-2010 operating at an accelerating voltage of 200 kV. A diluted NC solution in cyclohexanol (98.0%, Wako Pure Chemical) was trickled onto carbon-coated copper grids followed by drying in a vacuum overnight.

Results and Discussion

Ligand-Dependent Phase Determination of $CuInS_2$ NCs. For the reaction without amine addition, the product solution was turbid because of aggregation of the product powders, whereas a brown-colored transparent and colloidal solution was obtained for the reaction with the amine addition. This result shows that amine, HDA or OLA, acts as an effective surfactant to prevent aggregation and behaves as a capping reagent. In the FT-IR spectra of the product powders, in addition to the stretching and bending mode of N−H group of the amine, significant absorptions associated to the P−O vibration of the $P-O-C_8H_{17}$ group were detected. The results indicate that TOOP adsorbed on the NCs in addition to amines; and no TPOP adsorption was detected (see the Supporting Information). Therefore, the amines played the principal role in the capping of the NCs, but the TOOP had a small effect on the capping.

Figure 1 shows the XRD profiles of the $CuInS_2$ NCs extracted from the product colloidal solutions together with the calculated profiles of the chalcopyrite (CP), zincblende (ZB), and wurtzite (WZ) types of $CuInS_2$.[19,20] For the case using the HDA as a surfactant (panels a and b in Figure 1), a CP or ZB phase appeared when the storage time of the starting solution after the addition of the surfactant amine (t_{pres}) was 5 min. The difference between the CP and ZB phases appearing in XRD is very small. Therefore, we could not conclude whether the obtained phase was a CP or ZB phase. The subsequent optical results implied that a large number of defects, such as substitutional defects of copper at the indium site and indium at the copper site, were contained in the NCs; therefore, the phase was tentatively identified as the ZB phase in the present study, although additional experiments such as the Raman spectroscopy and detailed TEM observations are necessary for an accurate identification. When the t_{pres} was long as 3 h, the characteristic triplet at $2\theta \approx 27°$ and a distinct diffraction at $2\theta \approx 50°$ were clearly observed; the phase was definitely identified as the WZ phase by comparison of the calculated profiles. For the case using OLA as a surfactant, the phenomena similar to the HDA cases were observed. For instance, the ZB phase appeared at $t_{pres} = 5$ min, and the WZ phase appeared at $t_{pres} = 3$ h. These observations indicated that the observed phase was dependent on the t_{pres} of the starting solution after the addition of the surfactant amine; the short t_{pres} resulted in the ZB phase and the long t_{pres} resulted in the WZ phase. EDX analysis shows that the composition of the ZB and WZ phases, as shown in panels a and b in Figure 1 , are $X_{Cu}:X_{In}:X_S = 1.0:1.0:1.7$ and 1.0: 0.9:1.8, respectively. No significant composition difference is detected.

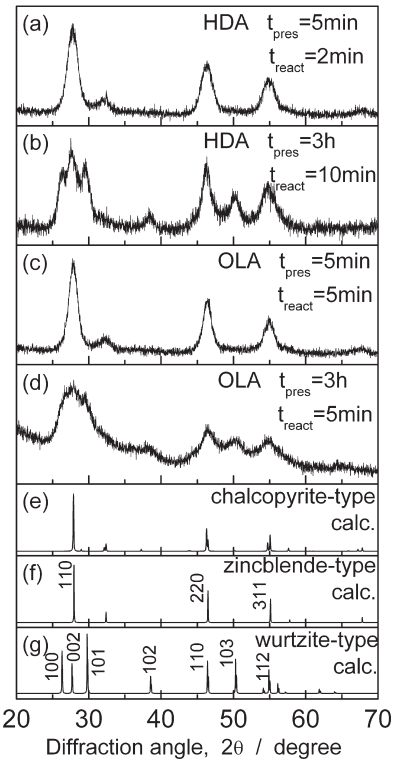

Figure 1. Observed XRD profiles of NCs extracted from the product colloidal solutions and calculated profiles of several $CuInS_2$ phases. The starting solutions were reacted at 200 °C. The additional surfactant amine, the reaction time, t_{react}, and the time since the addition of the surfactant, t_{pres}, were (a) hexadecylamine (HDA), $t_{pres} = 5$ min and $t_{react} = 2$ min; (b) HDA, $t_{pres} = 3$ h, and $t_{react} = 10$ min; (c) oleylamine (OLA), $t_{pres} = 5$ min, and $t_{react} = 5$ min; and (d) OLA, $t_{pres} = 3$ h, and $t_{react} = 5$ min. (e−g) Calculated XRD profiles of chalcopyrite-, zincblende- and wurtzite-type $CuInS_2$ phases, respectively. The chemical composition determined from EDX analysis of the ZB-type $CuInS_2$ (a) is $X_{Cu}:X_{In}:X_{In} = 1.0:1.0:1.7$ and the WZ-type $CuInS_2$ (b) is $X_{Cu}:X_{In}:X_{In} = 1.0:0.9:1.8$.

The structural transformation between the ZB and WZ phases dependent on the reaction conditions and the components of the reaction solutions are well-known phenomena in the synthesis of binary II−VI and III−V semiconductor NCs.[21−25] Similar to the very recent observations by Pan et al.,[18] we have found such a transformation in the ternary $I-III-VI_2$ semiconductor NCs. The raw materials of CuI and $InCl_3$ are soluble in both TOOP and amine, and the sulfur is soluble in both TPOP and amine. Therefore, the exchange of the complex ligand of the metallic monomers of CuI and $InCl_3$ and sulfur is possible by addition of the amine surfactant; the coordination of metallic monomers and sulfur were studied by IR spectroscopy. We first studied the IR spectra of the simple solutions of CuI and $InCl_3$ in TOOP and

(19) Abrahams, S. C.; Bernstein, J. L. *J. Chem. Phys.* **1973**, *59*, 5415.
(20) Guseinov, G. G.; Aliev, I. G.; Rzaev, S. S.; Aliev, O. M.; Aliev, F. I. *Neorg. Mater.* **1993**, *29*, 483.
(21) Qu, L.; Peng, X. *J. Am. Chem. Soc.* **2002**, *124*, 2049.
(22) Kim, Y.; Jun, Y.; Jun, B.; Lee, S.; Cheon, J. *J. Am. Chem. Soc.* **2002**, *124*, 13656.
(23) Yu, W. W.; Wang, Y. A.; Peng, X. *Chem. Mater.* **2003**, *15*, 4300.
(24) Li, Y.; Li, X.; Yang, C.; Li, Y. *J. Phys. Chem. B* **2004**, *108*, 16002.
(25) Cozzoli, P. D.; Manna, L.; Curri, M. L.; Kudera, S.; Giannini, C.; Striccoli, M.; Agostiano, A. *Chem. Mater.* **2006**, *17*, 1296.

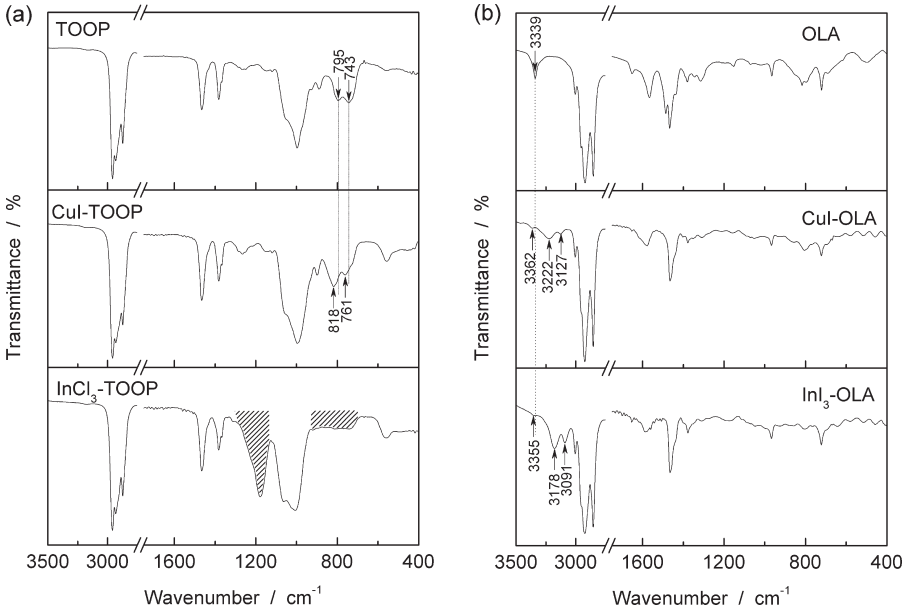

Figure 2. Infrared absorption spectra of (a) trioctylphosphite (TOOP) and its solutions of CuI and $InCl_3$ and (b) oleylamine (OLA) and its solutions of CuI and $InCl_3$.

OLA. Spectra a and b in Figure 2 show the IR spectra of the simple solutions of metallic monomers in TOOP and OLA. The top of Figure 2 a shows the spectrum of the pure TOOP. Absorption bands associated to the P−O vibration of the $P-O-C_8H_{17}$ group,[26,27] ν_{P-O}, was observed at 795 and 743 cm^{-1}. When CuI was dissolved in TOOP, the ν_{P-O} distinctly shifted ~20 cm^{-1} to a higher wavenumber. This blue shift should be attributable to the complexing of CuI with TOOP. For the $InCl_3$ in TOOP, a strong absorption band at ~1200 cm^{-1}, which was attributed to the stretching mode of O−P−O bond,[27,28] ν_{O-P-O}, and a broad absorption from 700 to 1000 cm^{-1}, which was attributable to ν_{P-O}, appeared because of coordination of $InCl_3$ with TOOP. For the OLA case (Figure 2 b), a distinct change upon dissolution of CuI or $InCl_3$ appeared above 3000 cm^{-1}, at which the stretching mode of the N−H bond,[29] ν_{N-H}, appeared. For the pure OLA, a single ν_{N-H} was observed at 3339 cm^{-1}. After dissolution of CuI or $InCl_3$, two ν_{N-H} bands at ~3200 and ~3100 cm^{-1} appeared. These bands are attributable to the coordination of CuI and $InCl_3$ with OLA.

Figure 3 a shows the IR spectrum of the TOOP solution of CuI and $InCl_3$, which corresponds to the reaction solution before the addition of the amine. A clear ν_{O-P-O} at ~1200 cm^{-1} (hatched area in the figure) for the $InCl_3$-TOOP complex and ν_{P-O} at 819 and 760 cm^{-1} for the CuI-TOOP complex were clearly observed. Therefore, it was obvious that the TOOP behaved as a complex ligand of metallic monomers in the solution before the addition of the amine. Figure 3 b shows the spectrum of the TOOP

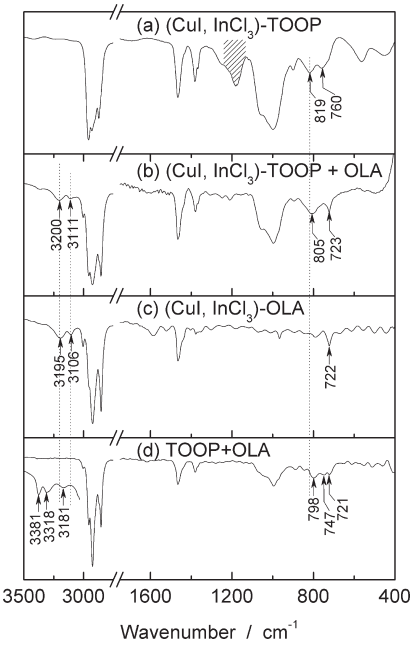

Figure 3. Infrared absorption spectra of (a) mixed solution of CuI and $InCl_3$ in TOOP ((CuI, $InCl_3$)-TOOP), (b) the mixed solution of (CuI, $InCl_3$)-TOOP and OLA 3 h after the addition of OLA, (c) mixed solution of CuI and $InCl_3$ in OLA ((CuI, $InCl_3$)-OLA), and (d) mixed solution of TOOP and OLA.

solution of the metallic monomers after the addition of OLA; the solution corresponds to the starting solution of the present $CuInS_2$ NCs synthesis. The ν_{O-P-O} at ~1200 cm^{-1} disappeared and ν_{N-H} at 3200 and 3111 cm^{-1} appeared by the OLA addition. The ν_{P-O} at ~820 and ~760 cm^{-1} before the OLA addition (Figure 3 a) shifted to ~800 and ~720 cm^{-1}, respectively, by the OLA addition. The disappearance of ν_{O-P-O} at ~1200 cm^{-1} and the red shift of the ν_{P-O} at ~820 and ~760 cm^{-1} were attributable to the dissociation of the bond of CuI and $InCl_3$ with TOOP. The appearance of ν_{N-H} at 3200 and 3111 cm^{-1} was attributable to the coordination of CuI and $InCl_3$ with

(26) Gay, I. D.; McFarlan, A. J.; Morrow, B. A. *J. Phys. Chem.* **1991**, *95*, 1360.
(27) Gordon, W. O.; Tissue, B. M.; Morris, J. R. *J. Phys. Chem. C* **2007**, *111*, 3233.
(28) Carauta, A. N. M.; Souza, V.; Hollauer, E.; Tellez, C. A. *Spectrochim. Acta A* **2004**, *60*, 41.
(29) The Aldrich Library of FT-IR Spectra, 2nd rd.; Aldrich: Milwaukee, WI, 1997.

OLA, because the ν_{N-H} at 3200 and 3111 cm^{-1} did not appear only by the mixing of OLA with TOOP as shown in Figure 3 d. These results indicated that the addition of the surfactant amine to the solution induced the ligand exchange of the metallic monomers from the TOOP to the OLA. Figure 4 shows the spectra concerning the sulfur component. Upon dissolution of the sulfur in TPOP, two new bands at 944 and 800 cm^{-1} (hatched area in Figure 4 b) appeared; the band at 944 cm^{-1} was attributed to the ν_{P-O}, and the band at 800 cm^{-1} was attributable to the stretching mode of the P=S bond,[29,31] $\nu_{P=S}$. The two newly appeared bands are evidence for the coordination of sulfur with TPOP. When OLA was added to the TPOP-S solution (Figure 4 e), these two bands remained and were clearly observed. This result indicated that the sulfur ligand did not change and remained as TPOP after addition of the amine to the reaction solution. Taking into consideration of that the electron donation ability of phosphorus in TPOP is smaller than TOOP and the metallic monomers used in the present synthesis behave as hard acid, it seems that the ligand exchange of metallic monomers from TOOP or OLA to TPOP by the mixing does not occur. On the basis of these IR results, we concluded that the structural transformation from the ZB to WZ phase dependent on the t_{pres} was caused by the ligand exchange of the metallic monomers, i.e., for the short t_{pres} of 5 min, and the $CuInS_2$ NCs formed by the reaction among the CuI-TOOP, $InCl_3$-TOOP, and S-TPOP complexes that resulted in the ZB phase. For the long t_{pres} of 3 h, the $CuInS_2$ NCs formed by the reaction among the CuI-OLA, $InCl_3$-OLA, and S-TPOP complexes that resulted in the WZ phase. Such an origin of the phase determination was consistent with that of the ZB-type $CuInS_2$ phase that appeared when no amine was added to the reaction solution, although the product was aggregated and was not a colloidal solution.

For the binary II−VI semiconductor NCs, such as ZnSe, ZnS and CdTe, the ligand-dependent phase determination of the ZB or WZ phase was also observed and studied from the viewpoint of the effects of the bond strength between the monomer and ligand molecule, i.e., ligand strength, on the nucleation and crystal growth rates.[23,24] We evaluated the nucleation and crystal growth behavior during the ZB or WZ phase formation from the XRD of the product NCs for various reaction times as shown in Figure 5. For the ZB phase formation, i.e., the complex ligand of the metallic monomers was TOOP, the NCs appeared after the short reaction time of 60 s; their average size gradually increased with an increase in the reaction time. This result indicated that the nucleation was fast and the growth was moderate during the ZB phase formation. For the WZ phase formation, i.e., the complex ligand of the metallic monomers was OLA, practically no product NCs were obtained for the 90 s reaction; this indicated the difficulty in the nucleation. Once the nucleation occurred, the NCs quickly grew; the

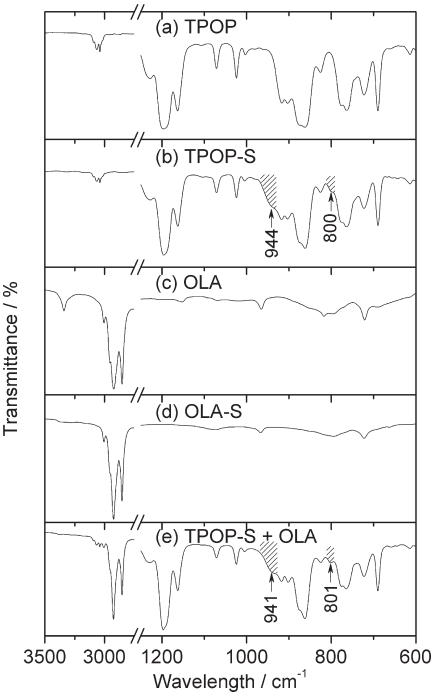

Figure 4. Infrared absorption spectra of (a) triphenylphosphite (TPOP), (b) sulfur solution in TPOP (TPOP-S), (c) OLA, (d) sulfur solution in OLA (OLA-S) and (e) the mixed solution of TPOP-S and OLA 3 h after the addition of OLA.

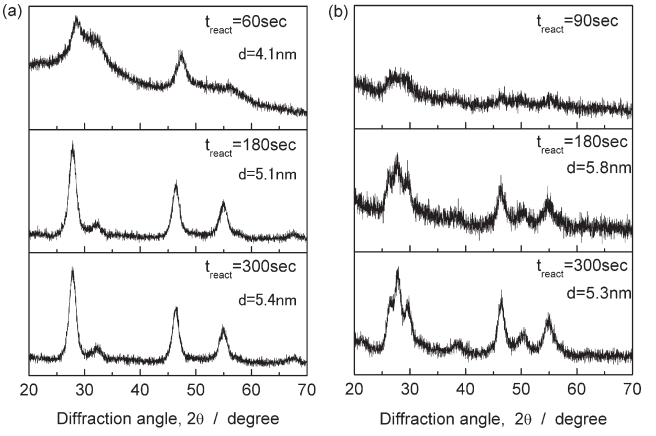

Figure 5. XRD profiles of the resulting NCs reacted at various times of (a) zincblende-type phase and (b) wurtzite-type phase. The zincblende-type phase was synthesized from the reaction solutions with 0.5 mmol OLA and their storage time t_{pres} was 5 min. The reaction temperature was 200 °C. The wurtzite-type phase was synthesized from the reaction solutions with 2.0 mmol OLA and their storage time t_{pres} was 5 min. The reaction temperature of 240 °C. *d* in the figure indicates the average particle size evaluated using Scherrer's formula.

average size evaluated from the XRD broadening was approximately the same between the NCs with 180 and 300 s of the reaction times. This observation indicated that the nucleation and growth rates of the WZ phase formation were respectively slower and higher than those of the ZB phase formation. The IR results indicated that the metallic monomers are strongly associated with the OLA rather than the TOOP; therefore, it was implied that the ligand strength between the monomers and TOOP is weaker than that between the monomer and OLA, because the complex ligand of the metallic monomers were exchanged from TOOP to OLA. On the basis of the

(30) Rossi, A.; Piras, F. M.; Kim, D.; Gellman, A. J.; Spencer, N. D. *Tribol. Lett*. **2006**, *23*, 197.
(31) Durig, J. R.; Johnson, R. D.; Nanaie, H.; Hizer, T. J. *J. Chem. Phys*. **1988**, *88*, 7317.

ligand strength of the TOOP and OLA, the nucleation and crystal growth observed in panels a and b in Figure 5 were explained as follows. When the complex ligand of the metallic monomer was TOOP, the nucleation was started and a large number of nuclei formed because of its weak ligand strength; and a large part of the metallic monomers was consumed during the nucleation. As a result, the concentration of remaining monomers became low in the growth period; therefore, the crystals gradually grew. On the contrary, when the complex ligand of the metallic monomer was OLA, nucleation was difficult due to high bond strength between the monomer and OLA; the consumption of the metallic monomer was very low during the nucleation. Therefore, the high growth rate was realized during the growth period, because a large amount of the metallic monomer remained after nucleation. For instance, the crystal growth was gradual and the thermodynamically stable CP or ZB phase[32,33] appeared when the TOOP coordinated with the metallic monomers. When the OLA was a complex ligand of the metallic monomers, because of the high monomer concentration during the growth period, the kinetically stable WZ phase[22,24,25,34,35] was formed. Such a situation during the $CuInS_2$ NCs formation was very similar to the ZB or WZ phase formation observed for the binary II−VI and III−V semiconductor NCs. For the ternary $CuInS_2$, the phase determination mechanism was understood by an explanation similar to the binary ZnSe, CdTe, and GaP. To synthesize a high-quality CP-type $CuInS_2$, which is the most thermodynamically stable phase, achieving a suppressed growth rate should be a key technique to prevent the formation of the kinetically stable WZ phase and substitutional defects of the metallic components.

Optical Properties of $CuInS_2$ and Core/Shell-Type $CuInS_2$/ZnS NCs. Figure 6 shows the optical absorption and PL spectra of the ZB- and WZ-type $CuInS_2$ NCs. The optical absorption spectra of both NCs had slight slopes; and the optical band gap of both phases were observed at 700−750 nm, which correspond to 1.65−1.77 eV in energy. The energy of 1.65−1.77 eV is distinctly greater than the bulk energy band gap of $CuInS_2$ (1.53 eV).[9] The higher optical band gap of the present NCs was attributed to the quantum size effect. The gently sloping absorption feature was attributed to the broad size distribution and the high defect density of the NCs.

A PL band centered at ~1000 nm was observed for the ZB-type NCs, although the center of the PL band for the WZ-type NCs was positioned at a wavelength longer than 1050 nm. Because the PL band was positioned far from the optical band gap of both phases of the NCs, i.e., a large Stokes' shift, the PL was not attributable to the exciton-recombination, but to the electron−hole recombination via defect levels as pointed out by Castro et al.[11] It was implied from the optical properties that the $CuInS_2$ NCs synthesized by the present method had a substantial concentration of substitutional defects such as copper at the indium site and indium at the copper site. To obtain the $CuInS_2$ NCs showing the PL due to the exciton recombination, it is necessary to improve the synthesis method and to use high-quality NCs.

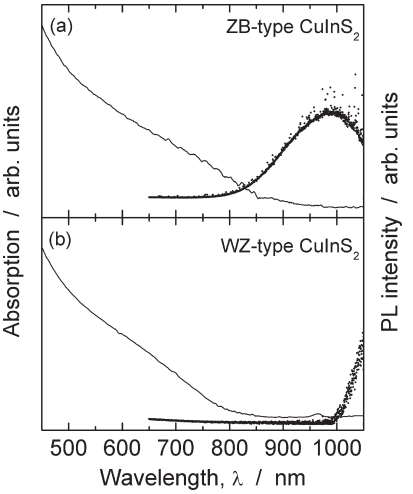

Figure 6. Optical absorption spectra and photoluminescence spectra of zincblende(ZB)- and wurtzite(WZ)-type $CuInS_2$ NCs. The zincblende-type NCs were synthesized at 200 °C for 120 s. from the starting solution containing 0.5 mmol of OLA and t_{pres} = 5 min, and wurtzite-type NCs were synthesized at 200 °C for 600 s from the starting solution containing 0.5 mmol of OLA and t_{pres} = 3 h.

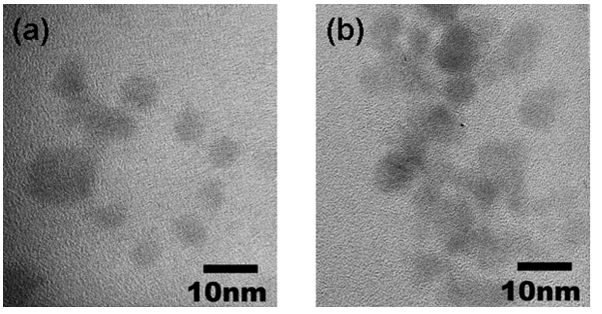

Figure 7. HREM images of NCs of (a) bare $CuInS_2$ NCs and (b) $CuInS_2$/ZnS core/shell NCs. The phase of the $CuInS_2$ NCs is the zincblende-type.

Figure 7 shows the HREM images of $CuInS_2$ and core/shell-type $CuInS_2$/ZnS; the phase of the $CuInS_2$ was the ZB-type. The average particle size of the bare and core/shell NCs evaluated from the images were 5.5 and 7.0 nm, respectively. Therefore, the thickness of the ZnS shell-layer was concluded to be ~1.2 nm. The optical absorption and PL spectra of these NCs are shown in Figure 8. For the core/shell NCs, the absorption was observed in the slightly shorter wavelength region than that of the $CuInS_2$ NCs. This observation may be attributable to the slight alloying between $CuInS_2$ and ZnS. The PL quantum yield (PLQY) evaluated by using Rhodamine 610 as a standard sample of the band at ~900 nm of the $CuInS_2$/ZnS core/shell NCs, which was attributable to the electron−hole recombination via defect levels, was ~2%,

(32) Binsma, J. J. M.; Giling, L. J.; Bloem, J. *J. Cryst. Growth* **1980**, *50*, 429.
(33) Chakvabarti, D. J.; Laughlin, D. E. *Bull. Alloy Phase Diag.* **1981**, *2*, 305.
(34) Yang, J. W.; Kuznia, J. N.; Chen, Q. C.; Khan, M. A.; Georg, T.; Graef, M. D.; Mahajan, S. *Appl. Phys. Lett.* **1995**, *67*, 3759.
(35) Narayanan, V.; Maharajan, S.; Sukidi, N.; Bachmann, K. J.; Woods, V.; Dietz, N. *Philos. Mag. A* **2000**, *80*, 555.

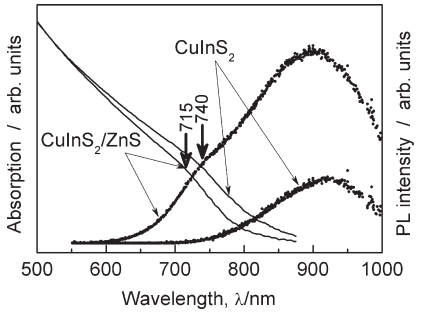

Figure 8. Optical absorption spectra and photoluminescence spectra of zincblende-type $CuInS_2$ and $CuInS_2$/ZnS core/shell NCs.

whereas the PLQY of the bare $CuInS_2$ NCs was under the detection limit, i.e., $< 0.2\%$ in our case. This indicated the effective passivation of the surfaces of the $CuInS_2$ NCs by the ZnS coating. Because the defect related emission at ~900 nm was observed after ZnS coating, the defect species in the interior and the size of the core $CuInS_2$ were approximately the same to those before ZnS coating. This indicated that the reaction between $CuInS_2$ and ZnS was significantly suppressed; therefore, the $CuInS_2$−ZnS alloy formed at the interface was concluded to be very small. It should be noted that a small shoulder at ~740 nm appeared in the PL spectrum of the core/shell NCs. The wavelength of the PL shoulder was very close to the optical band gap absorption at ~720 nm. The PL shoulder showing a small Stokes' shift was expected to be due to the exciton-recombination in the core $CuInS_2$ NCs. Because the exciton emission from $CuInS_2$ is very difficult to observe even for high-quality single crystals, it is more likely that the emission is attributable to the defect-related emission from $CuInS_2$−ZnS alloy formed at the interfaces between the core $CuInS_2$ and shell ZnS. However, the possibility of that the emission is attributable to the exciton recombination cannot be precluded completely at the present state, because the $CuInS_2$−ZnS alloy formed at the interface was very small. Further detailed study is necessary to attribute the emission to a small Stokes' shift.

Conclusion

We have studied the synthesis of the $CuInS_2$ and $CuInS_2$/ZnS core/shell NCs using simple and commercially available reagents as the starting materials and their optical properties. By using a starting solution preserved as long as 3 h after the addition of the surfactant amine, the obtained $CuInS_2$ phase was the WZ-type. On the other hand, the ZB-type $CuInS_2$ NCs were obtained by the immediate reaction after addition of the surfactant amine. This phase determination was explained by the thermodynamically stable CP or ZB phase appearing from the TOOP complex of metallic monomers; in this case, the crystal growth slowly occurred. The kinetically stable WZ phase appeared from the OLA or HDA complex of the metallic monomer; in this case, the growth rate was very fast.

Both the ZB- and WZ-type NCs showed a blue shift in the optical energy band gap due to the quantum size effect. A PL band was observed in the near-infrared region; the PL was attributable to the electron hole recombination via deep defect levels because its Stokes' shift was greater than 500 meV. It was noteworthy that a small shoulder appeared in the PL spectrum of the $CuInS_2$/ZnS core/shell NCs in addition to the deep level PL band; its Stokes' shift was ~50 meV. Although the possibility of that the emission is attributable to the exciton recombination cannot be precluded completely at the present state, it is likely that the emission is attributable to the defect-related emission from $CuInS_2$−ZnS alloy formed at the interfaces between the core $CuInS_2$ and shell ZnS taking into consideration that the exciton emission from $CuInS_2$ is very difficult to observe even for high quality single crystals. To replace the CdSe NCs by the $CuInS_2$ NCs, is strongly demanded that the synthesis method of the higher-quality and more defect-free $CuInS_2$ NCs with a chalcopyrite structure be established.

Acknowledgment. This work was supported in part by Grant-in-Aid for Scientific Research (B) from the Japan Society for the Promotion of Science (Grant 18360317 and 20360299).

Supporting Information Available: IR spectra of $CuInS_2$ NCs powders, on which the capping reagents of the NCs were determined; average particle size determined from the XRD (Figure 1) (PDF). This material is available free of charge via the Internet at http://pubs.acs.org.